6228
March 1, 2001
(T/E)

Minijet Corrections to Higgs Production

Vittorio Del Duca and Carl R. Schmidt*

Stanford Linear Accelerator Center
Stanford University, Stanford, California 94309

ABSTRACT

We study higher order corrections to Higgs production with an associated jet at SSC energies, using the resummation of the leading logarithmic contributions to multiple gluon emissions due to Lipatov and collaborators. We find a considerable enhancement of Higgs production at large transverse momenta.

Submitted to *Physical Review D*

PACS numbers: 14.80.Gt, 13.87.Ce, 12.40.Gg, 13.85.Qk

* Work supported by the Department of Energy, contract DE–AC03–76SF00515.

1. Introduction

One of the most important open questions in the Standard Model is the cause of the electroweak symmetry breaking. Both the SSC and the LHC are being built with the resolution of this puzzle in mind. The simplest explanation of the symmetry breaking is by a fundamental $SU(2)$ doublet scalar field, which leaves a neutral scalar, the Higgs boson, as a remnant of the symmetry breaking. This simple theory is the experimental standard against which any model of symmetry breaking will be measured. Thus, it is important that we completely understand the production environment of the Higgs boson at these hadron colliders.

At the SSC and the LHC, the Higgs boson is predominantly produced by gluon fusion. At lowest order α_s^2, it is produced with zero transverse momentum. The complete order α_s^3 corrections have been calculated[1] with an increase in the total cross section by a factor of 1.5 to 1.7. In addition, production of Higgs bosons with nonzero transverse momentum have been studied at order α_s^3. Higgs bosons produced with sizable $p_\perp$ may be phenomenologically important both in the intermediate mass region, where rare decay modes such as $\gamma\gamma$ and $\tau^+\tau^-$ must be used to observe the Higgs,[2] and for heavier Higgs bosons where the vector boson decay channels may be used.[3] At small transverse momentum it is necessary to resum large logarithms in $m_H^2/p_\perp^2$ in order to obtain a physical $p_\perp$ distribution.[4–6]

At the large center of mass energy $\sqrt{s}$ of the SSC and the LHC there are also important contributions from events with multiple final-state partons. These arise in a new kinematical region, the semihard region, characterized by scattering processes with $\sqrt{s}$ much larger than the momentum transfer Q, $s >> Q^2 >> \Lambda_{QCD}^2$. The study of this region is theoretically challenging because, in the perturbative expansion of cross sections, there appear coefficients containing logarithms of large ratios of kinematical invariants, of the order of the rapidity interval in the scattering process. In the inclusive production of the Higgs boson, the large ratios of kinematical invariants appear in the small-x evolution of the structure functions, thus requiring a more sophisticated analysis than the usual DGLAP evolution.[7]

In the context of jet production, Mueller and Navelet [8] were able to disentangle the small-x evolution of the structure functions from the appearance of large ratios of kinematical invariants in the parton subprocess by proposing to tag two jets at the extremes of the Lego plot in azimuthal angle and rapidity, with large transverse momenta $p_\perp$, and longitudinal momentum fractions x_A, x_B large enough that the parton structure functions could be computed from the ordinary DGLAP evolution. Thus, fixing the parton center of mass energy $\hat{s} = x_A x_B s$, the semihard region is realized also at the parton level $\hat{s} >> Q^2$, and the large logarithmic terms $\ln(\hat{s}/Q^2)$ appear in the parton cross section. To deal with these, Mueller and Navelet used the Balitsky-Fadin-Kuraev-Lipatov theory (BFKL),[9] which systematically resums the leading powers in the rapidity interval by using a multigluon amplitude where the rapidity interval between the *tagging jets* is filled with gluons, the *minijets*, whose spacing in rapidity is approximately uniform.

For the Higgs boson this program can be implemented by considering the production of the Higgs boson and a jet at the extremes of the Lego plot, with the rapidity interval between them filled with minijets, and the Higgs boson and the jet tagged at large transverse momenta. Since in gluon fusion the Higgs boson is produced via a quark loop, and the fermion-Higgs coupling is proportional to the quark mass, the only contribution to the quark loop which is numerically important is due to the top quark. Thus, two more scales, the Higgs boson and the top quark masses, enter the kinematics, and in order to avoid complications with the evolution of the structure functions[7] and apply the BFKL analysis, we must require that $\hat{s} >> p_\perp^2, m_H^2, m_t^2$. However, when $p_\perp^2 << m_H^2$ doubly logarithmic terms $\ln^2(m_H^2/p_\perp^2)$ appear, which more properly belong to the evolution of the structure functions[4–6] and may void the BFKL analysis. So in order to single out the strong rapidity-ordering regime characteristic of the BFKL analysis, the Higgs and the jet transverse momenta must be comparable to the Higgs mass $p_\perp^2 \simeq m_H^2$.

In section 2, we consider the inclusive production of the Higgs boson and a tagging jet, $p\,p \to H + \text{jet} + X$ in this kinematic situation. We recall the exact

Born-level calculation of Refs. 2 and 3 and consider its large-rapidity limit, and then we compute the leading logarithmic corrections at large rapidity, using the BFKL analysis. In section 3, we present numerical results for the inclusive Higgs-jet production, with or without integrating over the Higgs and jet transverse momenta, and compare the Born-level to the minijet-corrected calculations. Our conclusions are presented in section 4.

2. The Higgs + Jet Inclusive Cross section

We are going to study the semi-inclusive process $pp \to H + \text{jet} + X$ in the semihard regime defined by $\hat{s} >> Q^2$, with Q^2 being a typical momentum scale in the event, $Q^2 \approx m_H^2, m_t^2, p_\perp^2$. The tagging jet is required to ensure that we have an event with a large rapidity interval $y = y_J - y_H \approx \ln(\hat{s}/Q^2)$. Other relevant parameters in the event are the Higgs and jet transverse momenta $p_{H\perp}, p_{J\perp}$, their relative azimuthal angle ϕ and the average rapidity $\overline{y} = (y_J + y_H)/2$.

In the semihard, large-y regime we can write the cross section:

$$\frac{d\sigma}{dp_{H\perp}^2 dp_{J\perp}^2 d\phi dy d\overline{y}} \;=\; \sum_{ij} x_1 x_2 \, f_i(x_1) f_j(x_2) \, \frac{d\hat{\sigma}_{ij}}{dp_{H\perp}^2 dp_{J\perp}^2 d\phi} \; . \tag{2.1}$$

The parton subprocess cross section $d\hat{\sigma}_{ij}/dp_{H\perp}^2 dp_{J\perp}^2 d\phi$ contains the sum over all additional particles (i.e. minijets) in the event. The factorization of the minijets into the subprocess cross section is possible, because at large y the initial parton momentum fractions x_1 and x_2 are fixed in terms of the Higgs and jet momenta, and are essentially independent of the particles filling the rapidity interval. We will arrive at this cross section in several steps, starting with the exact Born level cross section, taking it to the $y >> 1$ limit, and finally filling in the rapidity interval with the minijets. Of course, the analysis can be applied equally well for $y << -1$, by reflecting along the beam axis.

i) Born Level Cross section. At the Born level the Higgs boson and the parton jet are produced back-to-back. The exact lowest order cross section can be put in

the form (2.1) with the replacement

$$\frac{d\hat{\sigma}_{ij}}{dp_{H\perp}^2 dp_{J\perp}^2 d\phi} \;\Rightarrow\; \frac{d\hat{\sigma}_{ij}}{d\hat{t}}\,\delta(p_{H\perp}^2 - p_{J\perp}^2)\,\delta(\phi-\pi)\;. \tag{2.2}$$

The parton momentum fractions and the subprocess invariants at this level are given by:

$$\begin{aligned} x_1 &= \frac{e^{\overline{y}}}{\sqrt{s}}(p_\perp e^{y/2} + m_{H\perp}e^{-y/2}) \\ x_2 &= \frac{e^{-\overline{y}}}{\sqrt{s}}(p_\perp e^{-y/2} + m_{H\perp}e^{y/2}) \\ \hat{s} &= x_1 x_2 s \;=\; p_\perp^2 + m_{H\perp}^2 + 2p_\perp m_{H\perp}\cosh(y) \\ \hat{t} &= -p_\perp^2 - p_\perp m_{H\perp}e^{-y} \\ \hat{u} &= -p_\perp^2 - p_\perp m_{H\perp}e^{y}\;, \end{aligned} \tag{2.3}$$

where $m_{H\perp} = (p_\perp^2 + m_H^2)^{1/2}$ and $p_\perp = p_{H\perp} = p_{J\perp}$. We use the lowest order Standard Model calculation for the subprocess cross sections $d\hat{\sigma}_{ij}/d\hat{t}$ in Ref. 2.

ii) Large-y Born Cross section. We now investigate the lowest order cross section when the rapidity interval y is large. For $y >> 1$ the lowest order amplitude is dominated by diagrams with gluon-exchange in the t-channel as in Fig. 1(a). In this limit the only subprocesses that contribute are $gg \to gH$ and $q(\overline{q})g \to q(\overline{q})H$. We obtain

$$\frac{d\hat{\sigma}_{gg}}{d\hat{t}} \;=\; C\,\frac{|\mathcal{F}(p_\perp^2)|^2}{p_\perp^2}\;, \tag{2.4}$$

where

$$C \;=\; \frac{N_c\alpha_s^3\alpha_W}{(N_c^2-1)128\pi M_W^2}\;. \tag{2.5}$$

Similarly, we find

$$\frac{d\hat{\sigma}_{qg}}{d\hat{t}} \;=\; \frac{d\hat{\sigma}_{\overline{q}g}}{d\hat{t}} \;=\; \frac{C_F}{C_A}\,\frac{d\hat{\sigma}_{gg}}{d\hat{t}}\;, \tag{2.6}$$

with $C_F/C_A = (N_c^2-1)/2N_c^2 = 4/9$ the ratio of the Casimir operators. The form factor $\mathcal{F}(p_\perp^2)$ is given in the appendix for both a scalar and a pseudoscalar Higgs

boson. We have checked that (2.4) agrees with previous results[5] if we take the additional limit $p_\perp^2 << m_H^2, m_t^2$. The parton momentum fractions in the large-y limit are

$$\begin{aligned} x_1 &= \frac{p_{J\perp}}{\sqrt{s}} e^{(\overline{y}+y/2)} = \frac{p_{J\perp}}{\sqrt{s}} e^{y_J} \\ x_2 &= \frac{m_{H\perp}}{\sqrt{s}} e^{(-\overline{y}+y/2)} = \frac{m_{H\perp}}{\sqrt{s}} e^{-y_H} \ . \end{aligned} \tag{2.7}$$

Equation (2.7) is also valid in the large-y limit when higher-order corrections are included, so that $p_{H\perp} \neq p_{J\perp}$.

iii) Minijet-corrected Cross section. As discussed in the introduction, going to higher orders in the coupling constant, i.e. to multiple parton emission, we encounter large logarithmic contributions. In the semihard regime, the BFKL theory[9] systematically resums the leading logarithmic terms $\ln(\hat{s}/p_\perp^2)$ by using a multigluon amplitude where the rapidity interval between the Higgs boson and the tagging jet is filled with gluons, strongly ordered in rapidity. This amplitude is shown in Fig. 1(b), where the thick line represents the resummation of the virtual radiative corrections, whose effect is to reggeize the gluons exchanged in the t channel. The real gluons are inserted on these using the Lipatov effective 3-gluon vertex.[9] The BFKL multigluon amplitude is then put in a rapidity-ordered phase space, the rapidities of the gluons are integrated out, and the dependence of the cross section on the gluon transverse momenta is reduced to the resolution of an integral equation. Its solution is then convoluted with the Higgs-boson production vertex on one side and the jet emission vertex on the other side of the rapidity interval to give the minijet-corrected parton cross section for producing the Higgs boson and a jet:

$$\frac{d\hat{\sigma}}{d^2p_{H\perp}d^2p_{J\perp}} = \frac{2C}{\pi} \frac{|\mathcal{F}(p_{H\perp}^2)|^2}{p_{J\perp}^2} f(y, p_{H\perp}, p_{J\perp}) \ . \tag{2.8}$$

In this equation $f(y, p_{H\perp}, p_{J\perp})$ is the Laplace transform in the rapidity interval y,

$$f(y, p_{H\perp}, p_{J\perp}) = \int \frac{d\omega}{2\pi i} e^{\omega y} f_\omega(p_{H\perp}, p_{J\perp}), \tag{2.9}$$

of the solution of the BFKL integral equation

$$f_\omega(p_{H\perp}, p_{J\perp}) = \frac{1}{(2\pi)^2} \sum_{n=-\infty}^{\infty} e^{in(\phi-\pi)} \int_{-\infty}^{\infty} d\nu \frac{(p_{H\perp}^2)^{-1/2+i\nu}(p_{J\perp}^2)^{-1/2-i\nu}}{\omega - \omega(n,\nu)}. \quad (2.10)$$

The eigenvalue of the integral equation $\omega(n,\nu)$ is

$$\omega(n,\nu) = \frac{2N_c\alpha_s}{\pi}\big[\psi(1) - Re\,\psi(\frac{|n|+1}{2} + i\nu)\big], \quad (2.11)$$

with ψ the logarithmic derivative of the Gamma function. Substituting (2.9) and (2.10) in (2.8), and doing the integral over ω, the minijet-corrected parton cross section becomes

$$\frac{d\hat{\sigma}}{dp_{H\perp}^2 dp_{J\perp}^2 d\phi} = \frac{C}{2\pi^2}\frac{|\mathcal{F}(p_{H\perp}^2)|^2}{p_{H\perp}\,p_{J\perp}^3} \sum_n e^{in(\phi-\pi)} \int_0^{\infty} d\nu e^{\omega(n,\nu)\,y} \cos\left(\nu\,\ln\frac{p_{H\perp}^2}{p_{J\perp}^2}\right). \quad (2.12)$$

If we integrate over the azimuthal angle ϕ in (2.12), only the $n = 0$ term survives.

iv) Minijet-corrected Cross section in the Saddle Point Approximation.

At very large values of the rapidity interval y, the correlations between the Higgs boson and the jet are washed out by the random walk in transverse momentum space of the gluons exchanged in the t channel. This can be seen most easily by evaluating (2.12) in the saddle-point approximation. The contribution of (2.11) to this equation is dominated by $n = 0$ and is strongly peaked near $\nu = 0$. Thus we keep only the first term in the Fourier expansion in ϕ, and expand $\omega(\nu) = \omega(0,\nu)$ about $\nu = 0$

$$\omega(\nu) = A - B\nu^2 + \cdots, \quad (2.13)$$

with

$$A = \frac{4N_c\alpha_s}{\pi}\ln 2, \quad B = \frac{14N_c\alpha_s}{\pi}\zeta(3). \quad (2.14)$$

Then we can evaluate (2.12) using the saddle-point approximation for the integral

over ν, to obtain

$$\frac{d\hat{\sigma}}{dp_{H\perp}^2 dp_{J\perp}^2 d\phi} = \frac{C}{4\pi}\,\frac{e^{A\,y}}{\sqrt{B\,\pi\,y}}\,\exp\left(-\frac{\ln^2(p_{H\perp}^2/p_{J\perp}^2)}{4By}\right)\,\frac{|\mathcal{F}(p_{H\perp}^2)|^2}{p_{H\perp}\,p_{J\perp}^3}. \tag{2.15}$$

The exponential growth of (2.15) with the rapidity interval y is due to the production of the minijets.

3. Numerical Results

We now examine numerically the effects of the minijets on Standard Model Higgs production at SSC energies. Throughout this section we will use a representative Higgs mass of 100 GeV and a top mass of 150 GeV, and the SSC center of mass energy $\sqrt{s} = 40$ TeV. The qualitative results do not depend strongly on these values of m_H and m_t. Except where indicated we set $\overline{y} = 0$ and observe the cross sections as a function of the rapidity interval $|y|$. We obtain a factor of two by including both positive and negative y. We use the "average" parton density functions of Diemoz *et al.*,[10] and we evaluate the QCD coupling α_s and the structure functions at a scale $Q^2 = m_H^2$. For $p_\perp > 50$ GeV and $|y| > 4$ the structure functions are always evaluated at $x > 10^{-2}$, so we are justified in using the DGLAP evolution in this region of phase space.

In Fig. 2 we present the inclusive Higgs-jet cross section, integrated over the azimuthal angle ϕ and over both transverse momenta with a cutoff of $p_{\perp\min} = 50$ GeV. We present it in the four approximations (*i-iv*) given in section 2. From the plot we see that the large-y Born cross section is a good approximation to the exact Born level cross section for $|y| \gtrsim 4$. The minijet-corrected cross section is typically enhanced over these lowest order cross sections by a factor of 2-3 for $|y| \gtrsim 4$. We define the K-factor as the ratio of the minijet-corrected cross section to the large-y Born cross section

$$K \;=\; \frac{d\sigma(\text{minijet})}{dy\,d\overline{y}} \Big/ \frac{d\sigma(\text{large}-y)}{dy\,d\overline{y}}, \tag{3.1}$$

and plot it in Fig. 3. K is defined so that $K \to 1$ as $y \to 0$. The minijet

enhancement is often plotted on a logarithmic scale[8]; on such a plot, the exact integral approaches the saddle point approximation, since the relative error tends to zero at large $\hat{s}$.

We next show the $p_\perp$ distributions of the Higgs and the tagging jet for rapidity intervals of $|y| = 4$ and $|y| = 8$ in Figs. 4(a) and 4(b), respectively. The other momentum is integrated over $p_\perp > p_{\perp\min} = 50$ GeV. Of course, for the Born cross section we have $p_{H\perp} = p_{J\perp}$, so the transverse momentum distributions of the Higgs and the jet are identical. However, with the inclusion of the minijets, this is no longer true. In fact the $p_{H\perp}$ distribution is considerably flatter than either the lowest order result or the minijet-corrected $p_{J\perp}$ distribution.

This effect can be understood by referring to Fig. 1(b) and analyzing the various terms in the minijet-corrected cross section (2.8). When convoluted with the structure functions we find

$$\sigma \;\approx\; \left[x_2 f(x_2)\Big|\frac{\mathcal{F}(p_{H\perp}^2)}{v}\Big|^2\right] f(y, p_{H\perp}, p_{J\perp}) \left[x_1 f(x_1)\Big(\frac{1}{p_{J\perp}}\Big)^2\right] , \qquad (3.2)$$

where the first bracketed term is associated with the Higgs boson production vertex and the last bracketed term is associated with the jet emission vertex. Note that the $1/p_{J\perp}^2$ comes from the jet vertex, whereas the form factor $\mathcal{F}(p_{H\perp}^2)$ is relatively constant in the region of interest. For very small rapidities we approach the Born cross section (2.4) with

$$f(y, p_{H\perp}, p_{J\perp}) \;\to\; \delta(p_{H\perp}^2 - p_{J\perp}^2)\,\delta(\phi - \pi) , \qquad (3.3)$$

so that both the Higgs boson and jet $p_\perp$ distributions fall as $1/p_\perp^2$. In addition, both x_1 and x_2 increase with $p_\perp$ via (2.7) so that there is an additional suppression from both parton density factors $(xf(x))^2$ as $p_\perp$ increases. However, for very large rapidities we have

$$f(y, p_{H\perp}, p_{J\perp}) \;\to \sim (p_{H\perp} p_{J\perp})^{-1} , \qquad (3.4)$$

and the Higgs boson and the tagging jet become uncorrelated. Now the Higgs boson distribution falls slower as $1/p_{H\perp}$, while the jet distribution falls faster as

$1/p_{J\perp}^3$. In addition both distributions are now only suppressed by one factor of $xf(x)$. These effects combine to strongly broaden the Higgs $p_\perp$ distribution. For the tagging jet the two effects tend to cancel and its $p_\perp$ distribution is much less modified.

Comparing Figs. 4(a) and (b), we can also observe some subtleties that have been neglected in the arguments of the last paragraph. For example, the separation between the Higgs and jet $p_\perp$ distributions at large $p_\perp$ shrinks as $|y|$ goes from 4 to 8. This is due to the fact that both quarks and gluons can enter the parton scattering on the jet side, while only gluons can enter on the Higgs side. Thus, the suppression from the structure functions is more severe on the Higgs side than on the jet side as x grows according to (2.7).

Finally, we discuss the effects of varying the Higgs and top-quark masses in the $p_\perp$ distributions of Fig. 4. Although the change in the contribution of the minijets is minor, there will still be some overall effects on the distributions. For example, because we have chosen the factorization and renormalization scales to be fixed at the Higgs mass, as m_H grows the coupling constant α_s and the structure functions become smaller, while the parton momentum fraction x increases. Consequently, the absolute scale of the $p_\perp$ distributions will decrease. Changing the top-quark mass has a different effect. The form factor $\mathcal{F}(p_{H\perp}^2)$ is roughly constant for $p_\perp \lesssim m_t$, but falls off as $m_t^2/p_\perp^2$ times logarithms for $p_\perp \gtrsim m_t$. Thus, while the jet $p_\perp$ distribution becomes independent of m_t at very large y, the Higgs and Born $p_\perp$ distributions fall more steeply for $p_\perp \gtrsim m_t$. For a given fixed $p_\perp$ larger than the top mass, the Higgs and Born $p_\perp$ distributions will increase with m_t.

The disappearence of correlations as $|y|$ increases can be seen dramatically in Fig. 5 where we plot the transverse momentum distribution of the tagging jet at a fixed Higgs transverse momentum of $p_{H\perp} = 125$ GeV. For a rapidity of $|y| = 2$ the cross section is strongly peaked near $p_{H\perp} = p_{J\perp}$. As the rapidity is increased there is a diffusion of the jet momentum away from the Higgs momentum until the peak disappears completely for $|y| = 8$. Note that the saddle point approximation

removes the correlation for all values of $|y|$. There is a similar diffusion of the azimuthal angle away from $\phi = \pi$ as the rapidity increases.

In Fig. 6 we consider the $p_{H\perp}$ distribution of centrally produced Higgs bosons. We fix $y_H = 0$ while integrating over the rapidity and transverse momentum of the tagging jet. The dashed line is the lowest order Born calculation with no cuts on the jet rapidity, while the dotdash line has a cut of $|y_J| > 4$. The jet transverse momentum is fixed at $p_{J\perp} = p_{H\perp}$ in these Born-level curves. The solid line is the minijet-corrected cross section with cuts of $|y_J| > 4$ and $p_{J\perp} > 50$ GeV. We apply these cuts in order to be confident that we are in a kinematical region where the minijet-corrected cross section is a good approximation. As in the previous plots we see that the minijet-corrected $p_{H\perp}$ distribution is much broader than the lowest order distribution. At $p_{H\perp} = 400$ GeV the minijet cross section with the kinematic cuts is over two orders of magnitude larger than the Born cross section with cuts. Moreover, it is almost within a factor of 2 of the lowest order Born cross section without any cuts at all.

4. Discussion and Conclusions

In this paper we have calculated the contribution of minijets to Higgs production in the semihard regime. The major phenomenological consequence of the minijets at SSC energies is to produce a substantial enhancement of Higgs bosons at large transverse momenta. Although our results are strictly valid for the semi-inclusive process $pp \to H + \text{jet} + X$ at large y, we have seen that these events may still make a sizable contribution to the inclusive process $pp \to H + X$ for large values of $p_{H\perp}$. The enhancement occurs because in the minijet-corrected cross section the falloff with $p_{H\perp}$ is much slower than the falloff with $p_{J\perp}$. This suggests that there may be a sizable contribution from events with a Higgs boson produced at large transverse momentum, balanced by the collective $p_\perp$ of several less energetic jets. These events should appear first at order α_s^4 in the $gg \to Hgg$ and $gq \to Hgq$ cross sections. The former has been calculated at the Born level in the large m_t

limit by Dawson and Kauffman,[11] who plotted the cross section with a single $p_\perp$ cutoff on both the outgoing gluons and the Higgs boson. It would be interesting to study this $gg \to Hgg$ cross section with the Higgs and gluon transverse momenta varied independently in order to check for an enhancement of events at large $p_{H\perp}$.

Acknowledgements

We wish to thank bj. Bjorken, Al Mueller, Michael Peskin, Wai-Keung Tang and Peter Zerwas for useful criticism and discussions.

APPENDIX

The analysis in this paper is valid both for a scalar Higgs boson and for a pseudoscalar Higgs boson, as would occur in two-Higgs-doublet models. The only change in our results is in the form factor $\mathcal{F}(p_\perp^2)$. We present the analytic form of $\mathcal{F}(p_\perp^2)$ in both cases below.

i) Scalar Higgs. The scalar Higgs coupling to the top quark is $-S(m_t/v)H\overline{\psi}\psi$, where S is a normalization constant which equals 1 for the Standard Model Higgs. The form factor is

$$\begin{aligned}\mathcal{F}_s(p_\perp^2) \;=\; S\left(\frac{4m_t^2}{m_{H\perp}^2}\right)\Bigg\{ -2 \,-\, \left(\frac{2p_\perp^2}{m_{H\perp}^2}\right)\Big[\sqrt{b}W(b) - \sqrt{a}W(a)\Big] \\ + \frac{1}{2}\Big(1 - \frac{4m_t^2}{m_{H\perp}^2}\Big)\Big[W(b)^2 - W(a)^2\Big]\Bigg\}\,,\end{aligned} \tag{A.1}$$

where $a = 1 + 4m_t^2/p_\perp^2$, $b = 1 - 4m_t^2/m_H^2$, and we take the root $\sqrt{b} = i\sqrt{|b|}$ for $b < 0$. We have also defined the function

$$W(c) \;=\; \begin{cases} -2i \arcsin\left(1/\sqrt{1-c}\right)\,, & c < 0 \\ \ln\dfrac{1+\sqrt{c}}{1-\sqrt{c}} \,-\, i\pi\,, & 0 < c < 1 \\ \ln\dfrac{\sqrt{c}+1}{\sqrt{c}-1}\,, & c > 1 \end{cases} \tag{A.2}$$

Note that $\mathcal{F}_s(p_\perp^2)$ is proportional to the form factor A_5 of Ref. 2 in the appropriate

kinematic channel. In the limit $p_\perp, m_H << m_t$, the form factor goes to the value $\mathcal{F}_s = -(4/3)S$.

ii) Pseudoscalar Higgs. The pseudoscalar Higgs coupling to the top quark is $-P(m_t/v)A\overline{\psi}i\gamma_5\psi$. In this case the form factor is

$$\mathcal{F}_p(p_\perp^2) \;=\; P\left(\frac{4m_t^2}{m_{H\perp}^2}\right)\left(-\frac{1}{2}\right)\Big[W(b)^2 - W(a)^2\Big] \;. \tag{A.3}$$

In the limit $p_\perp, m_H << m_t$, we find $\mathcal{F}_p = 2P$.

REFERENCES

1. S. Dawson, *Nucl. Phys.* **B359,** (1991) 283;
   A. Djouadi, M. Spira, and P.M. Zerwas, *Phys. Lett.* **B264,** (1991) 264;
   D. Graudenz, M. Spira, and P.M. Zerwas, *Phys. Rev. Lett.* **70,** (1993) 1372.
2. R.K. Ellis, I. Hinchliffe, M. Soldate, J.J. Van Der Bij, *Nucl. Phys.* **B297**, 221 (1988).
3. U. Baur and E.W.N. Glover, *Nucl. Phys.* **B339**, 38 (1990).
4. I. Hinchliffe and S.F. Novaes, *Phys. Rev.* **D38,** (1988) 3475.
5. R.P. Kauffman, *Phys. Rev.* **D44,** (1991) 1415; **D45,** (1992) 1512.
6. C.P. Yuan, *Phys. Lett.* **B283,** (1992) 395.
7. J.C. Collins and R.K. Ellis, *Nucl. Phys.* **B360** (1991) 3;
   S. Catani, M. Ciafaloni and F. Hautmann, *Nucl. Phys.* **B366** (1991) 135.
8. A.H. Mueller and H. Navelet, *Nucl. Phys.* **B282** (1987), 727.
9. L.N. Lipatov, *Sov. J. Nucl. Phys.* **23** (1976) 338;
   E.A. Kuraev, L.N. Lipatov and V.S. Fadin, *Sov. Phys. JETP* **44** (1976) 443, **45** (1977) 199;
   Ya. Ya. Balitskii and L.N. Lipatov, *Sov. J. Nucl. Phys.* **28** (1978) 822.
10. M. Diemoz, F. Ferroni, E. Longo, G. Martinelli, *Z. Phys.* **C39**, (1988) 21.
11. S. Dawson and R.P. Kauffman, *Phys. Rev. Lett.* **68,** (1992) 2273.

FIGURE CAPTIONS

1) Higgs + jet production amplitude in the large-y limit at (a) the Born level and (b) with minijet corrections.

2) Inclusive Higgs-jet production at the SSC, as a function of the rapidity interval y. The dashed and dotdashed lines are respectively the exact and large-y Born cross sections, the solid line is the minijet-corrected cross section, and the dotted line is the saddle point approximation to the solid line. The kinematic parameters are described in the text.

3) K-factor, as a function of the rapidity interval y. The solid line represents the ratio of the minijet-corrected cross section to the large-y Born cross section, and the dotted line is its saddle point approximation.

4) Higgs and jet $p_\perp$ distributions at (a) $|y| = 4$ and (b) $|y| = 8$. The dashed and dotdashed lines are respectively the $p_\perp$ distributions for the exact and the large-y Born cross section, for which $p_{H\perp} = p_{J\perp}$. The solid lines are the jet and Higgs $p_\perp$ distributions for the minijet-corrected cross section. Notice that in (b) the dashed and dotdashed lines completely overlap.

5) Jet $p_\perp$ distribution at a fixed Higgs transverse momentum of 125 GeV. From top to bottom, the solid lines are the jet $p_\perp$ distributions for the minijet-corrected cross section at $|y| = 2$, 4, 6 and 8. The dotted lines are the saddle point approximation to the solid lines.

6) Higgs $p_\perp$ distribution at $y_H = 0$. The dashed and dotdashed lines are the distributions for the exact Born cross section with, respectively, no cuts on the jet rapidity $|y_J|$, and $|y_J| > 4$. The solid line is the distribution for the minijet-corrected cross section with $|y_J| > 4$ and $p_{J\perp} > 50$ GeV.

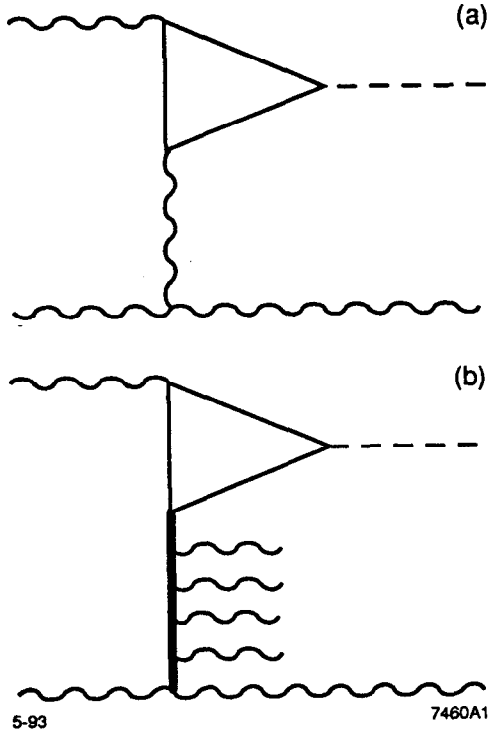

Fig. 1

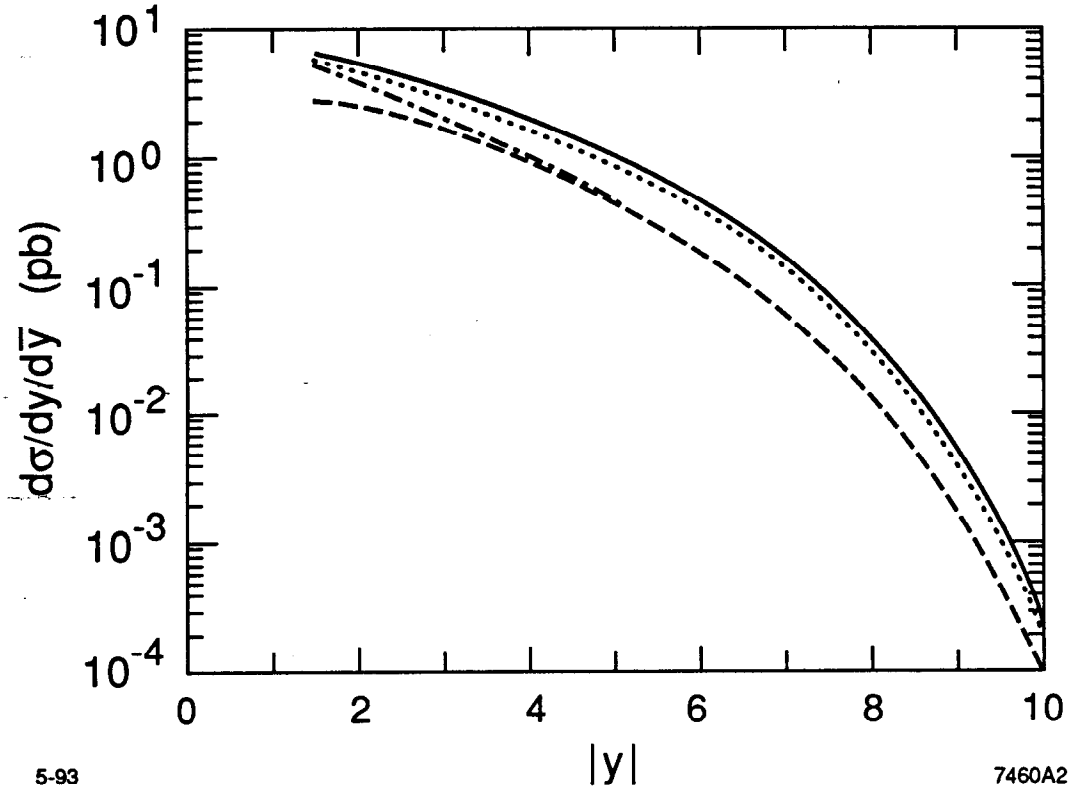
10^1
10^0
10^{-1}
10^{-2}
10^{-3}
10^{-4}
$d\sigma/dy/d\bar{y}$ (pb)
0
2
4
6
8
10
|y|
5-93
7460A2

Fig. 2

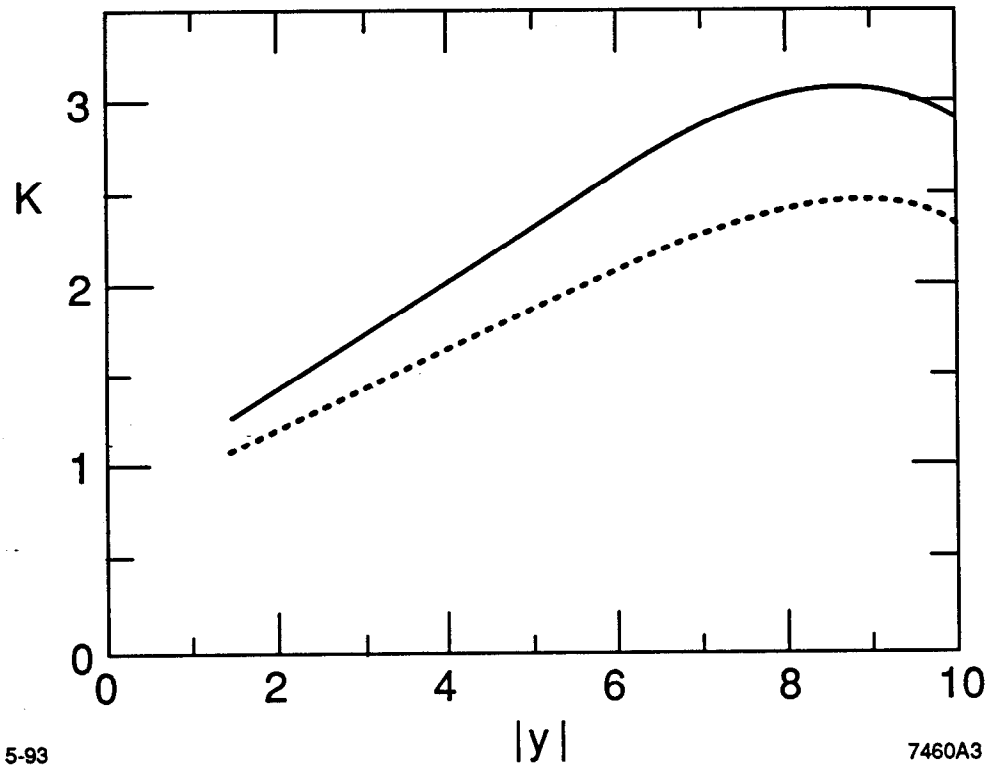

Fig. 3

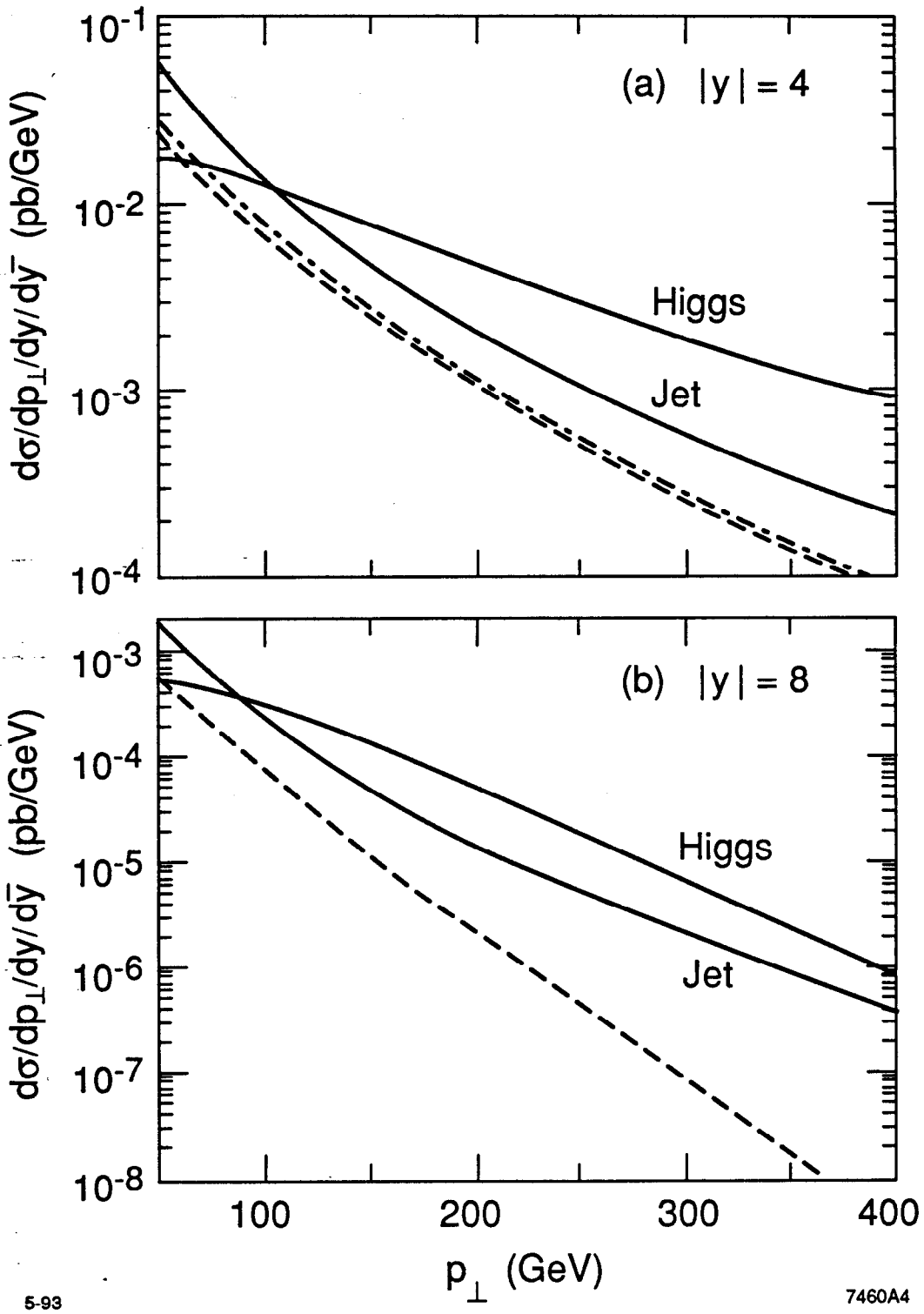
(a) |y| = 4
Higgs
Jet
(b) |y| = 8
Higgs
Jet
dσ/dp⊥/dy/dȳ (pb/GeV)
p⊥ (GeV)
10-1
10-2
10-3
10-4
10-5
10-6
10-7
10-8
100
200
300
400
5-93
7460A4

Fig. 4

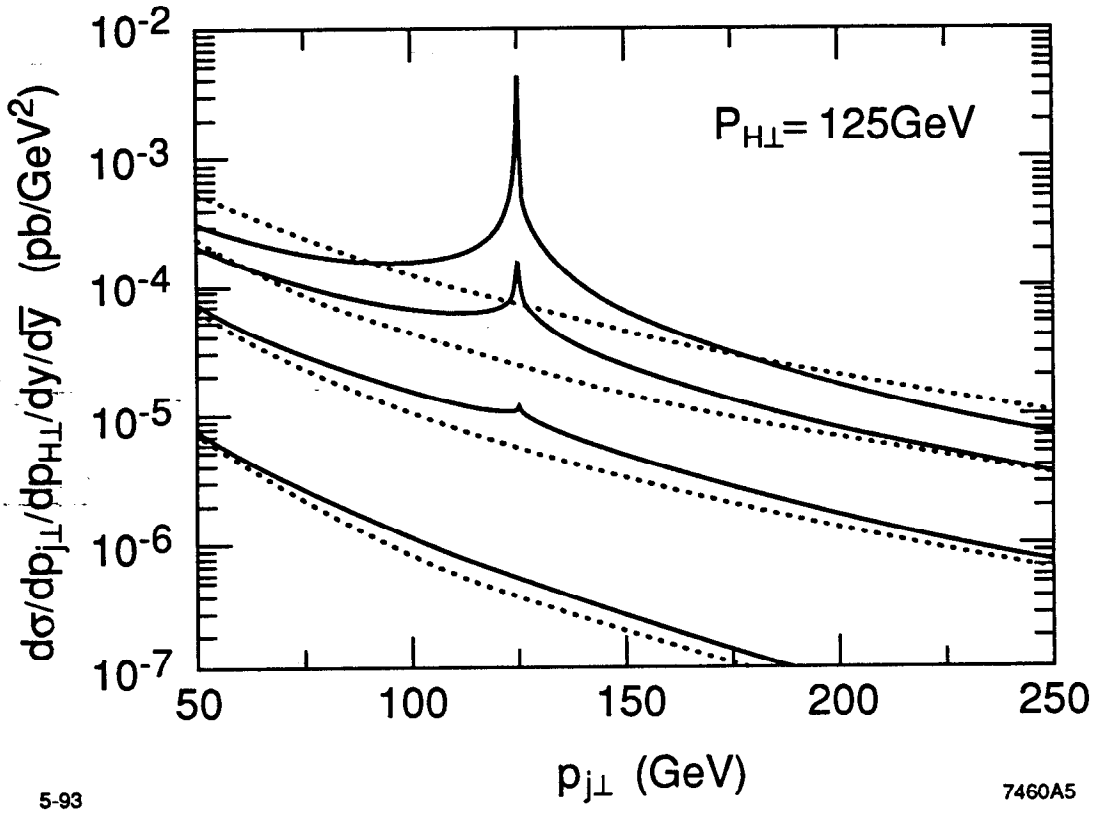
10^{-2}
10^{-3}
10^{-4}
10^{-5}
10^{-6}
10^{-7}
$d\sigma/dp_{j\perp}/dp_{H\perp}/dy/d\bar{y}$ (pb/GeV^2)
$P_{H\perp}$= 125GeV
50
100
150
200
250
$p_{j\perp}$ (GeV)
5-93
7460A5

Fig. 5

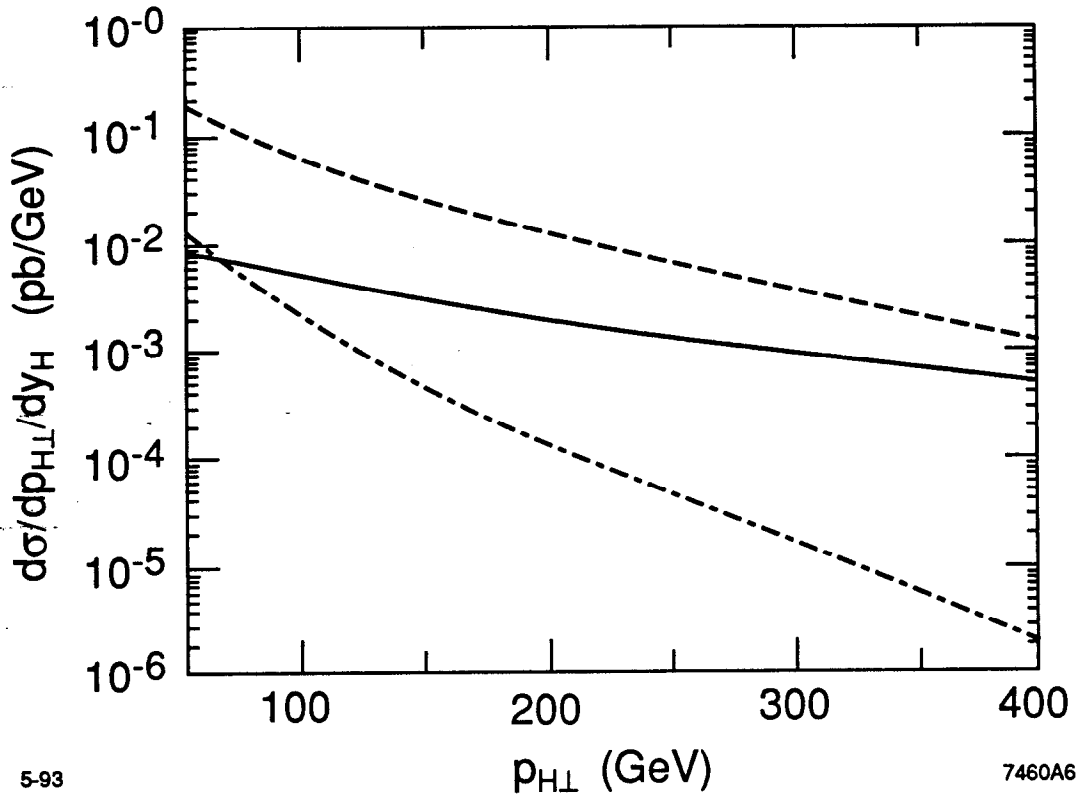
10^{-0}
10^{-1}
10^{-2}
10^{-3}
10^{-4}
10^{-5}
10^{-6}
$d\sigma/dp_{H\perp}/dy_H$ (pb/GeV)
100
200
300
400
$p_{H\perp}$ (GeV)
5-93
7460A6

Fig. 6